

Correlating Exciton Dynamics of Thermally Activated Delayed-Fluorescence Emitters to Efficiency Roll-Off in OLEDs

Monirul Hasan^{1,2}, Atul Shukla^{1,2}, Masashi Mamada³, Chihaya Adachi^{3,*}, Shih-Chun Lo^{1,2,4,†}, and Ebinazar B. Namdas^{1,2,‡}

¹*School of Mathematics and Physics, The University of Queensland, Brisbane, QLD 4072, Australia*

²*Centre for Organic Photonics & Electronics, The University of Queensland, Brisbane, QLD 4072, Australia*

³*Center for Organic Photonics and Electronics Research, Kyushu University, Fukuoka 819-0395, Japan*

⁴*School of Chemistry and Molecular Biosciences, The University of Queensland, Brisbane, QLD 4072, Australia*

(Received 27 April 2022; revised 10 October 2022; accepted 17 October 2022; published 28 November 2022)

Physical parameters, such as decay rates and photoluminescence (PL) quantum efficiencies, associated with thermally activated delayed fluorescence (TADF) emitters play a critical role in determining the performance of organic light-emitting diodes (OLEDs). Herein, we investigate the impact of TADF decay rates and PL quantum efficiencies on external quantum efficiency (EQE) roll-off. Our analysis reveals that a high EQE with suppressed efficiency roll-off in TADF OLEDs can be achieved by shortening the delayed lifetime with an increasing delayed contribution or by shortening the prompt lifetime with increasing prompt contribution simultaneously. We further show that TADF compounds with long delayed and/or prompt lifetimes can give rise to multiple spin cycling and subsequently result in significant exciton quenching and efficiency roll-off in OLEDs. These results provide universal selection criteria for TADF emitters in OLEDs to concurrently achieve a high maximum EQE and low-efficiency roll-off.

DOI: 10.1103/PhysRevApplied.18.054082

I. INTRODUCTION

Organic semiconductors exhibit many novel physical, electrical, and optical properties, which provide benefits not typically available in conventional inorganic semiconductors. Some examples include the capacity for large-area solution processing, mechanical flexibility, and almost unlimited availability of chemical structures due to the ease of organic synthesis. As a result, organic light-emitting diodes (OLEDs) based on organic semiconductor materials have always attracted widespread interest in both academia and industry [1–3]. However, one of the critical challenges in the field of OLED technology is the reduction of efficiency at high current densities, commonly known as efficiency roll-off. OLEDs preserving high efficiency at a high brightness level (typically $>5000 \text{ cd m}^{-2}$) are indispensable for many applications, such as general illumination, picoprojectors, virtual reality, augmented reality, and biomedical devices [4–6]. Due to the efficient roll-off in OLEDs, to achieve a high brightness level, often a high current density is required, which not only increases the power consumption but also reduces the device lifetime, and therefore, limits the scope for commercial applications.

In recent years, OLEDs with thermally activated delayed fluorescence (TADF) emitters [7–18] have received considerable attention due to their low manufacturing cost as an alternative to heavy-metal-based phosphorescent OLEDs. TADF emitters utilize the reverse intersystem crossing (RISC) process to harvest triplet excitons to achieve a maximum internal quantum efficiency close to 100% by converting triplets into singlet excitons. However, OLEDs fabricated with TADF emitters frequently exhibit extensive external quantum efficiency (EQE) roll-off due to long delayed lifetimes (usually on the order of 1–100 μs) arising from the RISC process. These long delayed lifetimes can lead to triplet accumulation under high current injection conditions in OLEDs, resulting in enhanced bimolecular interactions such as exciton-polaron [19–21] and exciton-exciton annihilations [22,23], and subsequently EQE roll-off. Improving the RISC rate via reducing the singlet (S_1) and triplet (T_1) states energy gap (ΔE_{ST}) [17,24–27] or enhancing spin-orbit coupling (SOC) [28–32] are regarded as crucial strategies to suppress efficiency roll-off in TADF OLEDs. However, it would be ideal for widespread practical implementation if a correlation between the intrinsic photophysical parameters of a TADF emitter [i.e., decay rates and their respective photoluminescence (PL) quantum efficiencies] and EQE roll-off could be established.

Herein, various TADF PL decays are generated and investigated by tuning the exciton decay rates and PL

*adachi@cstf.kyushu-u.ac.jp

†s.lo@uq.edu.au

‡e.namdas@uq.edu.au

quantum efficiencies to understand their impact on EQE roll-off. Our results reveal that not only the RISC rate but also the radiative decay rate of singlet excitons and the relative contribution of prompt and delayed efficiencies can significantly influence the TADF emission and EQE roll-off characteristics in OLEDs. Through comprehensive numerical studies on 240 TADF systems, it is shown that a high peak EQE and a low EQE roll-off in TADF OLEDs can be achieved primarily via two general strategies: (1) shortening the delayed lifetime with increasing delayed contribution, or (2) shortening the prompt lifetime with increasing prompt contribution. We experimentally demonstrate the validity of our theoretical results from steady-state and time-resolved electroluminescence (EL) measurements. These results provide the necessary criteria for the screening of materials and designing benchmarks for promising TADF emitters for high-efficiency and low-efficiency roll-off OLEDs.

II. THEORY AND NUMERICAL MODEL

The nature of the TADF process is governed by the PL quantum efficiencies and decay rate constants, once ΔE_{ST} is small enough to trigger the upconversion from triplet to singlet states [7,32–35], as shown in Fig. 1. By assuming a negligible nonradiative decay rate from the singlet state, the PL quantum efficiencies and decay rate constants in a three-level TADF model can be formulated as

$$\phi_P = \frac{\tau_P A_P}{\tau_P A_P + \tau_D A_D} \phi_{PL}, \quad (1)$$

$$\phi_D = \frac{\tau_D A_D}{\tau_P A_P + \tau_D A_D} \phi_{PL}, \quad (2)$$

$$k_S = k_P \phi_P, \quad (3)$$

$$k_{ISC} = k_P \phi_{ISC}, \quad (4)$$

$$k_{RISC} = k_D \frac{\phi_{RISC}}{1 - \phi_{ISC}}, \quad (5)$$

$$k_T = k_D - \phi_P k_{RISC}, \quad (6)$$

where ϕ_{PL} , ϕ_P , ϕ_D , ϕ_{ISC} , and ϕ_{RISC} are the total, prompt, delayed, intersystem crossing (ISC), and RISC PL quantum efficiencies, respectively; A_P and A_D are the amplitudes of prompt and delayed components, respectively; τ_P and τ_D are the prompt and delayed lifetimes, respectively; $k_P = 1/\tau_P$ and $k_D = 1/\tau_D$ represent the prompt and delayed PL decay rates, respectively; k_S , k_{ISC} , k_{RISC} , and k_T are the radiative singlet decay rate constant from the singlet excited state to the ground state, ISC rate constant from the singlet excited state to the triplet excited state, RISC rate constant from the triplet excited state to the singlet excited state, and nonradiative decay rate constant from the triplet excited state to the ground state, respectively. For such a TADF compound doped in a host matrix (shown in

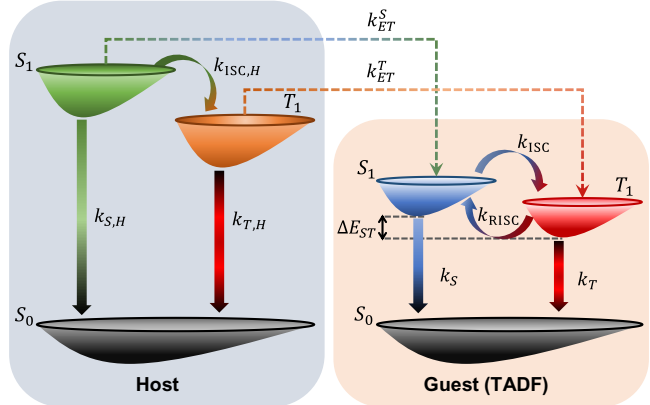


FIG. 1. Basic energy diagram for a host-guest (TADF as the guest) system, assuming a three-state process for both host and guest TADF emitter.

Fig. 1), the time evolution of the exciton densities under optical pumping can be formulated by the following rate equations:

$$\frac{dS_H}{dt} = G - (k_{S,H} + k_{ISC,H} + k_{ET}^S) S_H, \quad (7)$$

$$\frac{dT_H}{dt} = k_{ISC,H} S_H - (k_{T,H} + k_{ET}^T) T_H, \quad (8)$$

$$\frac{dS_G}{dt} = k_{ET}^S S_H + k_{RISC} T_G - (k_S + k_{ISC}) S_G, \quad (9)$$

$$\frac{dT_G}{dt} = k_{ET}^T T_H + k_{ISC} S_G - (k_{RISC} + k_T) T_G, \quad (10)$$

where G is the exciton-generation rate; S_H , T_H , S_G , and T_G are the singlet and triplet exciton densities of host and guest, respectively; $k_{S,H}$, $k_{ISC,H}$, and $k_{T,H}$ are the host radiative singlet decay rate, ISC rate, and nonradiative decay rate from the triplet excited state, respectively; k_{ET}^S and k_{ET}^T are the energy-transfer rate from the host singlet excited state to the guest singlet excited state and the host triplet excited state to the guest triplet excited state, respectively.

To study the impact of the TADF decay rates and quantum efficiencies in the EQE roll-off process, we generate various excited-state PL decays for TADF systems by employing Eqs. (1)–(10). The generated decays are categorized into six cases with 40 TADF systems in each case by tuning only the TADF (guest) decay rate constants (i.e., k_S , k_{ISC} , k_{RISC} , and k_T) and PL quantum efficiencies (i.e., ϕ_P , ϕ_D , ϕ_{ISC} , and ϕ_{RISC}). For all generated TADF decays in this study, ϕ_{PL} is taken as constant and equal to the experimental PL quantum yield (PLQY) of about 84% of a model TADF system, 5 wt % 2,4,5,6-tetra(9H-carbazol-9-yl)isophthalonitrile (4CzIPN) doped in 1,3-bis(*N*-carbazolyl)benzene (mCP), as reported previously [21]. The decay rate constants for the host are either

taken from the literature [36,37] or calculated from experimental data (see Note 1 and Table S1 within the Supplemental Material [38]) and kept constant for all generated decays. Considering a perfectly charge-balanced OLED with a uniform distribution of excitons and polarons, the EQE response can be calculated for each generated decay as [21,22,33,39],

$$\frac{dP}{dt} = \frac{J(t)}{qd} - \gamma P^2, \quad (11)$$

$$\frac{dS_H}{dt} = \alpha P^2 - (k_{S,H} + k_{ISC,H} + k_{ET}^S)S_H, \quad (12)$$

$$\frac{dT_H}{dt} = (1 - \alpha)P^2 + k_{ISC,H}S_H - (k_{T,H} + k_{ET}^T)T_H, \quad (13)$$

$$\begin{aligned} \frac{dS_G}{dt} &= k_{ET}^S S_H + k_{RISC} T_G - (k_S + k_{ISC})S_G \\ &\quad - k_{SP} S_G P - k_{ST} S_G T_G + \frac{\alpha}{2} k_{TT} T_G^2, \end{aligned} \quad (14)$$

$$\begin{aligned} \frac{dT_G}{dt} &= k_{ET}^T T_H + k_{ISC} S_G - (k_{RISC} + k_T)T_G \\ &\quad - k_{TP} T_G P - \frac{1 + \alpha}{2} k_{TT} T_G^2, \end{aligned} \quad (15)$$

$$\eta_{\max} = [\alpha\phi_P + \{\alpha(1 - \phi_P) + (1 - \alpha)\}\phi_{RISC}] \eta_{\text{out}}, \quad (16)$$

$$\eta(J) = \eta_{\max} \frac{S(t = \infty, J)}{S_0}, \quad (17)$$

where P and J are the polaron and current densities, respectively; $\gamma = q(\mu_h + \mu_e)/(\varepsilon_r \varepsilon_0)$ is the Langevin recombination rate; q is the elementary charge; d is the width of the recombination zone, which is assumed to be 15 nm in this study [21,40,41]; ε_0 and ε_r are the permittivity of free space and the relative permittivity, respectively; α is the singlet generation ratio and is assumed to be 0.25, in accordance with the spin statistics; μ_h (μ_e) is the hole (electron) mobility of the emissive layer; k_{SP} , k_{ST} , k_{TP} , and k_{TT} refer to the rate constants of singlet-polaron (SPA), singlet-triplet (STA), triplet-polaron (TPA), and triplet-triplet annihilation (TTA), respectively; η_{out} ($\approx 20\%$) is the light out-coupling efficiency, η_{\max} is the theoretical maximum EQE; and S_0 is the singlet density without any annihilation processes. Previous studies have indicated that joule heating or heat-induced quenching can induce EQE roll-off in fluorescent OLEDs [42,43]. In our study, the impact of joule heating is not considered, as the rate of heat-induced quenching in TADF materials is not reported yet. For each generated TADF decay, the EQE response as a function of current density is calculated by selecting k_S , k_{ISC} , k_{RISC} , k_T , and η_{\max} for each generated TADF decay using Eqs. (11)–(17). All the other parameters are taken as constants from the literature [40,44,45] and listed in Tables S1 and S2 within the Supplemental Material [38].

It is important to note that a simple rate-equation model and constant-exciton annihilation rates are considered to calculate the EQE response and transient EL for each generated TADF decay. Therefore, any variations in calculated EQEs and transient EL response are only due to the change in the intrinsic TADF decay rates and their quantum efficiencies. However, actual device behaviors and annihilation rates depend on several factors and can significantly impact the degree of EQE roll-off and the shape of transient ELs, as previously reported [46–49]. Our analysis provides an estimation of EQE roll-off and transient ELs, where only the variations in the photophysical parameters associated with the TADF process are considered.

III. RESULTS AND DISCUSSION

A. EQE roll-off characteristics

Figure 2 shows two cases of generated TADF decay characteristics with 5 wt % 4CzIPN:mCP as the

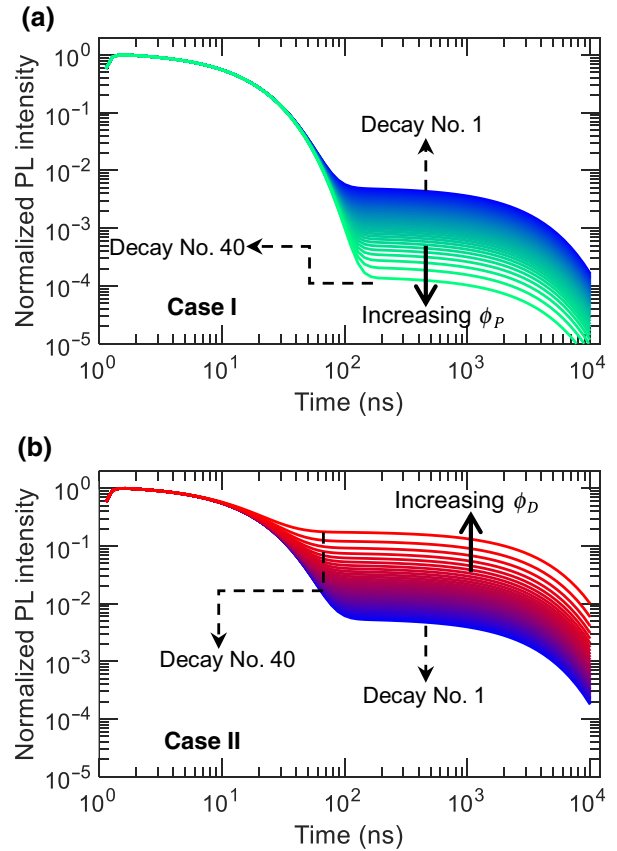


FIG. 2. TADF process and generated TADF decays for Cases I and II. (a) Case I with increasing prompt efficiency, while $\phi_P > \phi_D$. (b) Case II with increasing delayed efficiency, while $\phi_D > \phi_P$. Solid arrows represent the change in PL decays due to the tuning of ϕ_P and ϕ_D for Case I and Case II, respectively; and dashed arrows indicate the first and final index of generated PL decays.

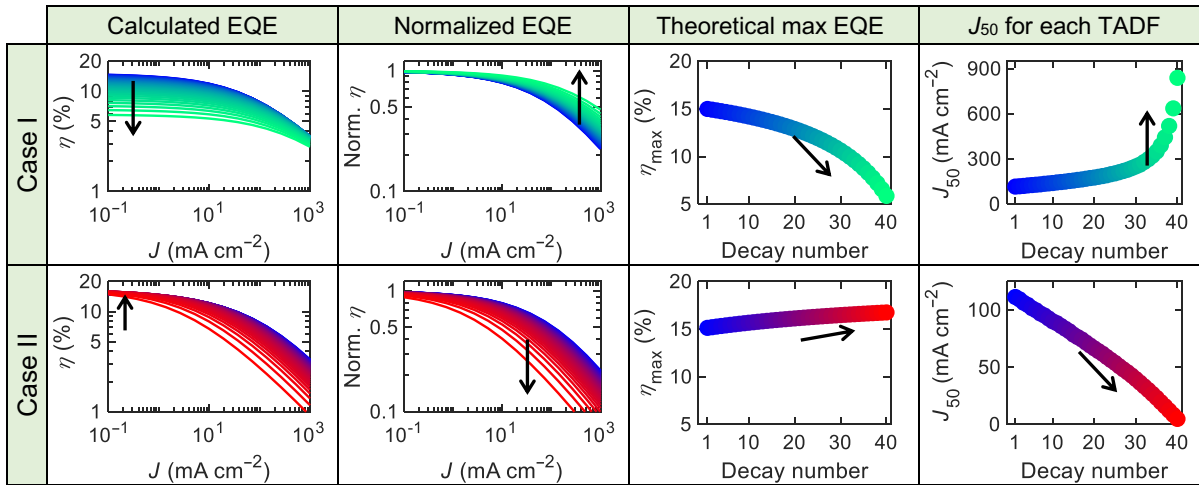


FIG. 3. EQE roll-off characteristics for Cases I and II. Calculated EQE response and normalized EQE as a function of current density, theoretical maximum EQE, and estimated J_{50} for each TADF process for Case I (top row) and Case II (bottom row). Solid arrows represent the changes due to variations in decay rates.

standard, where each PL decay corresponds to an individual TADF molecule. In Case I, ϕ_P is linearly increased from 43% to 82% and, consequently, ϕ_D is reduced from 41% to 2%, while all the lifetimes are kept constant for all decays, as reported previously ($\tau_P = 14$ ns, $\tau_D = 2.9 \mu\text{s}$) [21]. Similarly, a reverse process with increasing ϕ_D and decreasing ϕ_P is taken into consideration for Case II. Figure S1 within the Supplemental Material [38] shows the corresponding decay rates; PL quantum efficiencies; amplitudes of prompt and delayed components; lifetimes; and spin cycling (\bar{n}), which is defined as the average number of $S_1 \rightarrow T_1 \rightarrow S_1$ cycles [50], respectively, for each decay scheme of Cases I and II. It is observed for Case I that the increase in ϕ_P results in a decrease in k_{RISC} and an increase in k_S . Conversely, in Case II, the increase in k_{RISC} and the decrease in k_S can be observed due to the gradual increase of ϕ_D . The decays in Cases I and II are used to investigate the impact of prompt and delayed efficiencies on the EQE roll-off process.

To understand the EQE roll-off behaviors in OLEDs in both cases, we calculate (1) the EQE response as a function of current density, (2) the critical current density (J_{50}) at which the calculated EQE becomes half of its maximum value, and (3) the theoretical maximum EQE, using Eqs. (11)–(17) for each TADF process (as shown in Fig. 3). In Case I, it is noticeable that the EQE roll-off is suppressed, and the corresponding J_{50} values increase with increasing ϕ_P , although there is a drop in the theoretical maximum EQEs as the contribution from the delayed component is reduced with the gradual reduction of ϕ_D and \bar{n} . This indicates that the decrease in spin cycling can reduce the EQE roll-off, although the tuning in Case I results in a reduction of the maximum EQEs in this model. However, compounds with nearly 100% ϕ_{PL} (i.e., with negligible

nonradiative losses) can suppress this reduction of maximum EQEs, as experimentally demonstrated by Kaji *et al.* [51] and Kondo *et al.* [52] previously. Conversely, the opposite trend is observed for the EQE response of Case II. A gradual decrease in J_{50} is observed for Case II, indicating a high EQE roll-off, although the increase in ϕ_D greatly improves the theoretical maximum EQE. Interestingly, for Case II, the increase in k_{RISC} results in high EQE roll-off behaviors, as the delayed fluorescence becomes stronger with an increase in spin cycling and reduced singlet radiative rate. Combining the EQE roll-off trends in Cases I and II, it is clear that prompt and delayed efficiencies, or, in other words, spin cycling, play a critical role in the EQE roll-off process and an enhancement in k_{RISC} values does not necessarily reduce EQE roll-off in TADF OLEDs.

The efficiency of TADF emitters also largely depends on the prompt and delayed lifetimes. To observe the effect of lifetimes on EQE behaviors, we generate PL decay traces for Cases III and IV with a gradual change in prompt and delayed lifetimes, respectively, as shown in Fig. 4, where the amplitude of prompt and delayed components remains constant for each decay. In Case III, the prompt lifetime is decreased from 100 to 2.5 ns, while the delayed lifetime is constant, and in Case IV, the delayed lifetime is decreased from 16.4 to 0.8 μs , while the prompt lifetime is constant. Figure S2 within the Supplemental Material [38] shows the corresponding decay rates, quantum efficiencies, amplitudes, lifetimes, and spin cycling for each decay of Cases III and IV, respectively. For Case III, a gradual decrease in the prompt lifetime with a constant delayed lifetime gives rise to k_S and k_{ISC} . Additionally, as the total PL quantum yield is the same for all TADF decays, an increase in k_{ISC} induces a slight increase in k_{RISC} and a reduction in k_T . Similarly, an increase in k_{ISC}

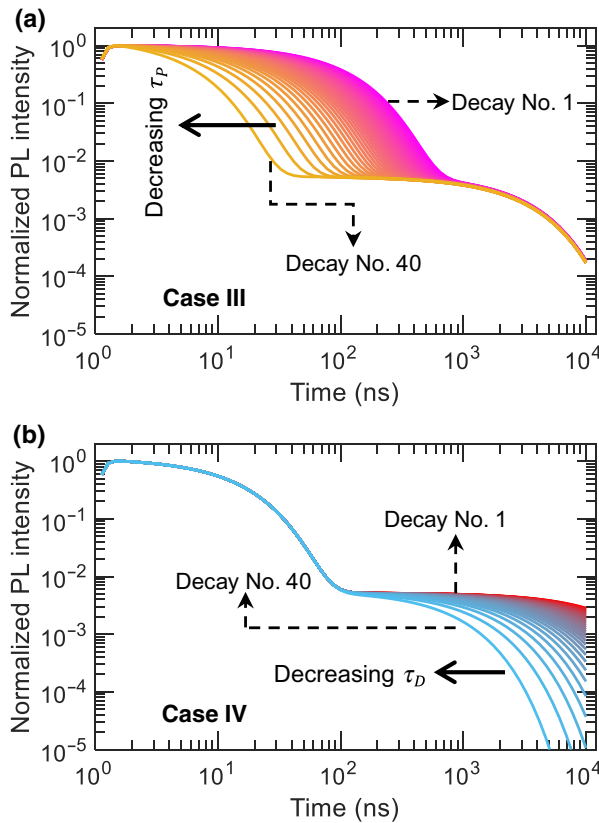


FIG. 4. Generated TADF decays for Cases III and IV. (a) Case III with decreasing prompt lifetime, while the delayed lifetime remains the same for each decay. (b) Case IV with decreasing delayed lifetime, while the prompt lifetime remains the same for each decay. Solid arrows represent the change in PL decays due to the tuning of τ_p and τ_D for Case III and Case IV, respectively; and dashed arrows indicate the first and final index of generated PL decays.

and k_{RISC} can be seen in Case IV with the decrease in the delayed lifetime. In terms of EQE roll-off characteristics, both cases show improvement in the EQE roll-off and a gradual increase in J_{50} (shown in Fig. 5). Note that, in Case III, the EQE roll-off is reduced as the prompt-fluorescence process becomes faster, although the spin-cycling number is increasing, which is opposite to the Case II conditions. However, in Case IV, a reduction in the delayed lifetime increases ϕ_p (similar to Case I) and makes the delayed-fluorescence process faster, which reduces EQE roll-off. In addition, for Case IV, a slight decrease in the theoretical maximum EQE is observed, as shortening the delayed lifetime causes a decrease in the contribution from the delayed component due to an increment in k_T .

Finally, we generate Cases V and VI, where we vary both the lifetime and amplitude of the prompt and delayed components simultaneously, as shown in Fig. 6, to find the conditions that can produce a low EQE roll-off while preserving a high theoretical maximum EQE in TADF OLEDs. For Case V, τ_p is reduced from 100 to 2.5 ns,

and A_p is increased from 0.94 to 0.99 in such a way that τ_p , ϕ_p , and ϕ_D remain the same for each decay (see Fig. S3 within the Supplemental Material [38]). Similarly, the delayed lifetime is reduced, and the amplitude of the delayed component is increased for Case VI (see Fig. S3 within the Supplemental Material [38]). Consequently, in Case V, a gradual increase in k_S and k_{ISC} can be observed, while k_{RISC} and k_T remain the same for all decays. In Case VI, a gradual increase in k_{RISC} and k_T can be observed, while k_S and k_{ISC} remain the same for all decays. In both cases, there is an improvement in EQE roll-off behaviors with no drop in the theoretical maximum EQE values (Fig. 7). These results suggest that EQE roll-off can be significantly reduced while preserving high maximum EQEs in OLEDs by tuning either the prompt or delayed components following the approach of either Case V or Case VI.

Case V highlights maximizing the contribution from the prompt component, which can be facilitated by a short prompt lifetime and a high amplitude of the prompt component. Organoboron-based 5,9-diphenyl-5,9-diaza-13 b-boranaphtho [3,2,1-de] anthracene (DABNA)-type TADF molecules with multiple resonance effects usually exhibit behavior similar to Case V and are reported to show a low efficiency roll-off [52–55]. In contrast, Case IV highlights that maximizing the RISC rate by shortening the delayed lifetime and increasing the delayed contribution can also be effective at reducing efficiency roll-off. Recent studies suggest that reducing the energy gap between charge-transfer (CT) singlet (${}^1\text{CT}$) and triplet (${}^3\text{CT}$) states, and maximizing spin-orbit coupling between excited states with different spin multiplicities, i.e., nonadiabatic vibronic coupling between ${}^1\text{CT}$ and locally excited triplet (${}^3\text{LE}$) states, can greatly improve the RISC rate [32]. Therefore, TADF molecules with near-degenerate ${}^1\text{CT}$, ${}^3\text{CT}$, and ${}^3\text{LE}$ (${}^1\text{CT} \approx {}^3\text{LE} \approx {}^3\text{CT}$) states may show similar behavior to that described for Case VI. Previously, controlling the thorough-space distance between donor and acceptor [35] and the inclusion of multiple donor moieties to form charge-resonance-type hybrid triplet states [56] have proven to be highly effective strategies to maximize the RISC rate.

B. Transient electroluminescence

The shape of the transient EL provides critical insights into the exciton annihilation process and EQE roll-off in TADF OLEDs. To observe the variation of the EL transient in different cases considered in this study, we calculate the singlet densities as a function of time for a 10- μs electrical pulse using Eqs. (11)–(15). The calculated singlet densities, which can be assumed as representative of the EL transients, are shown in Fig. 8 for Cases I–VI (all the parameters used to calculate the transient ELs are summarized in Tables S1 and S2 within the Supplemental Material

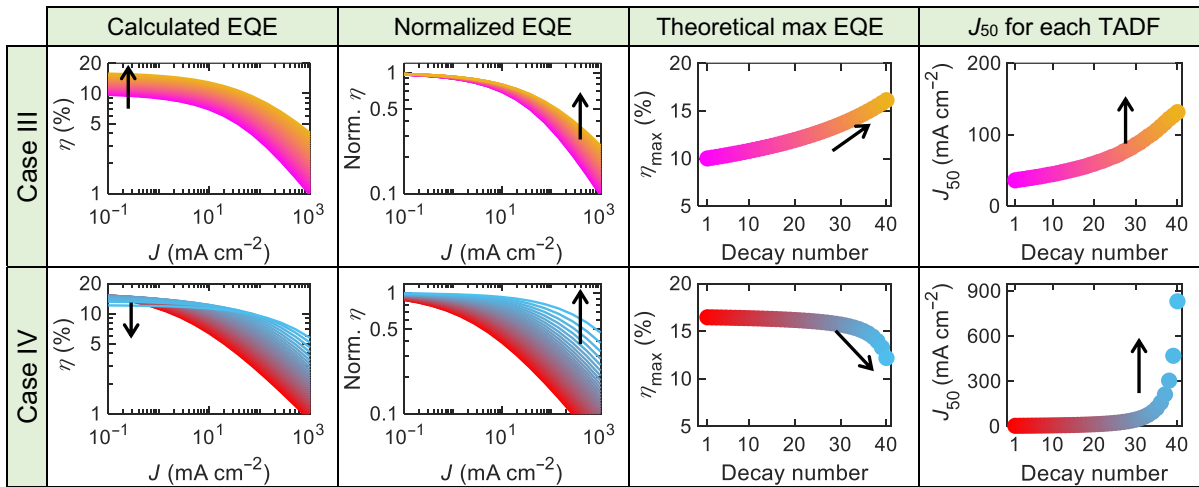


FIG. 5. EQE roll-off characteristics for Cases III and IV. Calculated EQE response and normalized EQE as a function of current density, theoretical maximum EQE, and estimated J_{50} for each TADF process for Case III (top row) and Case IV (bottom row). Solid arrows represent changes due to variations in decay rates.

[38]). For each case, we consider two conditions: (1) without any annihilations when STA, SPA, TTA, and TPA processes are ignored, by taking the corresponding annihilation rate constants as zero in Eqs. (14) and (15); and (2) with annihilation when all the annihilation processes are considered in Eqs. (14) and (15). These two conditions allow us to observe how annihilation processes modify the shape of EL transients in six generated cases. Note that all the EL transients are calculated at a high current density of 100 mA cm^{-2} , as the impact of annihilation is usually more prominent under high current densities.

For Case I, it is evident from the normalized ELs that, with a gradual decrease in spin cycling, the EL transients reach saturation on a shorter timescale and start to resemble more the ELs of fluorescent materials [57–59]. Interestingly, when ϕ_P is equal to the total quantum yield and ϕ_D is zero, it produces a decay similar to a conventional pure fluorescent compound with a lifetime of the prompt component, as shown in Fig. S4 within the Supplemental Material [38]. Conversely, in Case II, the ELs reach saturation on a longer timescale as the increase in spin cycling makes the exciton deactivation process slower. This indicates that TADF processes in Case II are moving more toward the direction of pure phosphorescence-type emissions [60–62] with microsecond lifetimes. In addition, due to the higher relative contribution of triplets, the absolute singlet density or EL intensity is gradually increasing for Case II, and the opposite can be seen for Case I. This also supports the change in the theoretical maximum EQE under steady-state conditions for Cases I and II. Furthermore, comparing normalized EL transients with and without annihilation in Case II, it is observed that TADFs with higher ϕ_D reach saturation much faster under annihilation conditions. Note that annihilation processes

can significantly modify the EL transient shape in such a way that it can reach saturation faster [58,63,64]. Since triplet-based annihilation processes are the dominant loss mechanisms for Case II, this leads to EL transients reaching early saturation with higher ϕ_D under annihilation conditions.

In Case III, the increase in k_S , k_{ISC} , and k_{RISC} and the decrease in k_T induce a high triplet contribution. Since the exciton relaxing via the triplet-to-singlet upconversion channel takes a longer time than the direct relaxation from the singlet state, the transient ELs reach saturation slower with a decrease of the prompt lifetime. However, the impact of annihilation is more significant on TADF processes with longer prompt lifetimes. This can be seen by comparing EL transients with and without annihilation conditions. In Case IV, the decrease in delayed lifetime greatly impacts on the transient ELs reaching saturation faster. Although a decrease in singlet density can be observed due to an increase in k_T , the impact of annihilation in TADFs with longer delayed lifetimes is higher, as their EL intensities shift to saturation faster under annihilation conditions compared to those without annihilation conditions.

For Case V, the prompt lifetimes and amplitudes in each decay are tuned in such a way that the prompt and delayed contributions remain the same for each TADF process. As a consequence, the change among EL transients without annihilation is minimal compared to all the other cases. Additionally, TADF processes with longer prompt lifetimes and lower prompt amplitudes contribute more to annihilation processes, which lead to faster saturation. Similar to Case V, the prompt and delayed efficiencies remain the same in Case VI, although TADF processes with shorter delayed lifetimes and higher delayed

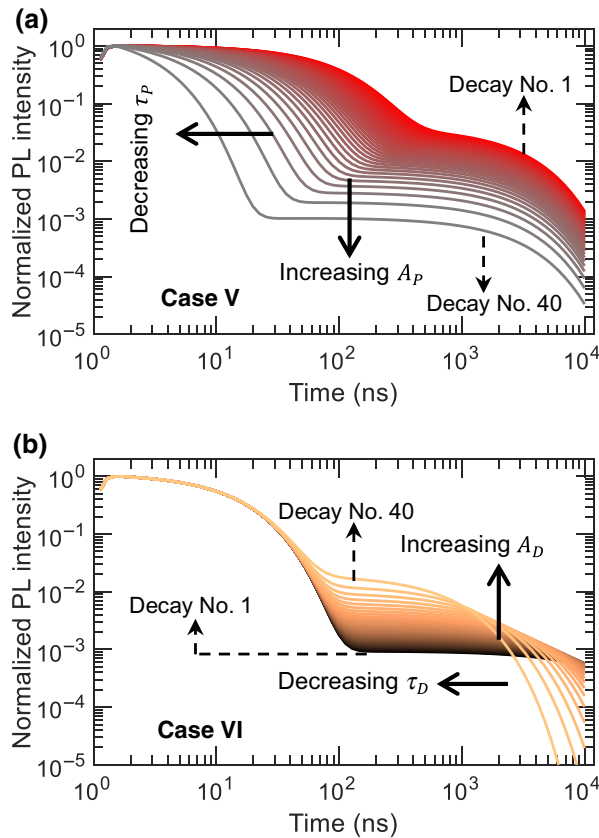


FIG. 6. Generated TADF decays for Cases V and VI. (a) Case V with decreasing prompt lifetime and increasing prompt amplitude. (b) Case VI with decreasing delayed lifetime and increasing delayed amplitude. Solid arrows represent the change in PL decays due to the tuning of τ_p and A_p for Case V; and τ_D and A_D for Case VI. Dashed arrows indicate the first and final index of generated PL decays.

amplitudes contribute to the faster rise in EL transients for Case VI. This indicates that the gradual change in transient EL shapes can be attributed to the faster TADF process due to tuning in the Case VI rather than due to annihilation processes. Furthermore, a gradual increase in singlet densities can be seen both with and without annihilation, as there is no decrease in the contribution from triplet states, unlike in Case IV.

C. Experimental implementation

The results in previous sections emphasize that EQE roll-off depends on different photophysical parameters not only on ISC and RISC rates. Here, we select two TADF materials, 4CzIPN and 2,4,6-tri[4-(10H-phenoxazin-10H-yl)phenyl]-1,3,5-triazineto (tri-PXZ-TRZ) [65,66], to study their PL and EL properties. Figures 9(a) and S5 within the Supplemental Material [38] show the photophysical properties of TADF blend films in mCP host with 5 wt% TADF dopant. The calculated decay rate constants and PL quantum efficiencies from photophysical

measurements are listed in Table I. Note that their photophysical properties resemble the Case IV conditions closely, as the delayed lifetime of tri-PXZ-TRZ is shorter than that of 4CzIPN. To study the EL properties, OLEDs are fabricated by employing the same TADF blends as the emissive layer using the following device structure: indium tin oxide (ITO, 100 nm)/poly(3,4-ethylenedioxythiophene):poly(styrenesulfonate) (PEDOT: PSS, ~40 nm)/mCP:5 wt% TADF(~30 nm)/3,3',5,5'-tetra[(*m*-pyridyl)phen-3-yl]biphenyl (BP4mPY, 60 nm)/LiF(1 nm)/Al(100 nm), in which ITO, PEDOT:PSS, BP4mPY, and LiF/Al are used as anode, hole-transport layer, electron-transport layer, and cathode, respectively (see Fig. S6 within the Supplemental Material [38]). The device structures of the OLEDs for both compounds are the same (e.g., the thickness of all layers), which allows us to study device properties under almost identical conditions. To investigate the EQE roll-off in the OLEDs, we measure the current-density–voltage–luminance (see Fig. S7 within the Supplemental Material [38]) and EQE–current-density properties [Fig. 9(b)]. A detailed comparison of the device properties is summarized in Table S3 within the Supplemental Material [38]. From the EQE–current-density plots, it is notable that devices with tri-PXZ-TRZ show lower EQE roll-off with significantly higher experimental J_{50} values compared to those of 4CzIPN-based devices. This is in line with the EQE response of Case IV, as discussed in earlier sections. Interestingly, the rates of ISC and RISC are comparable for both compounds, although the nonradiative k_T is almost 1 order of magnitude higher for tri-PXZ-TRZ (see Table I). As a consequence, ϕ_D and \bar{n} are lower for tri-PXZ-TRZ compared to 4CzIPN, which suggests suppression of the EQE roll-off in tri-PXZ-TRZ-based OLEDs, which is evident from Case IV. The experimental peak EQE (see Table S3 within the Supplemental Material [38]) is higher for 4CzIPN-based devices compared to that of tri-PXZ-TRZ-based devices, as the total quantum yield and calculated theoretical maximum EQE are higher in the case of 4CzIPN. To further understand the EQE roll-off process in both compounds, we estimate EQE responses using the decay rates from Table I and annihilation rates from Table S2 within the Supplemental Material [38], as shown in Fig. S8 within the Supplemental Material [38]. A low efficiency roll-off is observed for tri-PXZ-TRZ similar to the experimental EQE responses. It is important to note that the prompt lifetime of tri-PXZ-TRZ is slightly longer than that of 4CzIPN, although this variance is not high enough to cause an effect similar to that of Case III. Nevertheless, these results highlight that two compounds with comparable ISC and RISC rates can show different degrees of EQE roll-off, depending on the relative contributions from prompt and delayed fluorescence.

Experimental transient EL responses from the OLEDs are obtained by applying a 10-μs voltage pulse. Figure 9(c) shows the EL transient and corresponding EL decay

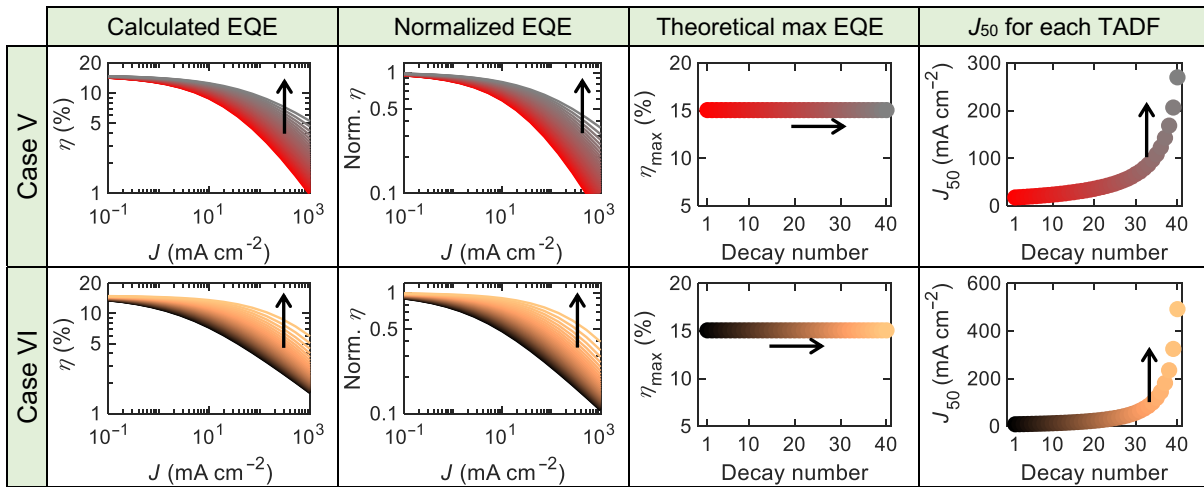


FIG. 7. EQE roll-off characteristics for Cases V and VI. Calculated EQE response and normalized EQE as a function of current density, theoretical maximum EQE, and J_{50} for each TADF process for Case V (top row) and Case VI (bottom row). Solid arrows represent changes due to variations in decay rates.

collected at a high current density of about 1 A cm^{-2} . The EL transient from tri-PXZ-TRZ reaches saturation on a shorter timescale than that of 4CzIPN. This trend is expected, as the delayed-fluorescence process is faster for tri-PXZ-TRZ and observed in the calculated EL responses in Case IV (Fig. 8). Moreover, the EL transient of tri-PXZ-TRZ shows less change when compared to the theoretical EL response [calculated from the parameters in Table I using Eqs. (11)–(15), without considering any annihilation processes], which supports the suppressed efficiency roll-off in tri-PXZ-TRZ-based OLEDs under steady-state conditions (see Fig. S9 within the Supplemental Material [38]). A shorter-lived EL decay is also observed for tri-PXZ-TRZ, which can be predicted from the theoretically calculated EL decays, as shown in Fig. 8 for Case IV. It is important to mention that there might be a possibility that different annihilation rate constants, electron and hole mobilities in the emissive layer, and energy-level alignment of the emitters in tri-PXZ-TRZ- and 4CzIPN-based OLEDs can produce minor differences in steady-state and transient EL properties between them [67–71]. However, we believe that the impact of these operations is insignificant compared to the intrinsic TADF properties of dopants.

To further validate our studies with experimental results, we analyze a series of carbazole-benzonitrile (CzBN) derivatives reported by Hosokai *et al.* [72]

previously. The photophysical parameters for 5CzBN, 4CzBN, *p*-3CzBN, *o*-3CzBN, and *m*-3CzBN doped in 2,8-bis(diphenylphosphoryl)dibenzo[*b,d*]thiophene (PPT) host are shown in Fig. S10 and listed in Table S4 within the Supplemental Material [38]. Figure S11 within the Supplemental Material [38] shows the EQE–current-density plots and experimental J_{50} values for each compound (details on the device structure and fabrication can be found in the original paper [72]). Although a weak delayed fluorescence ($\phi_D \approx 0$) in doped films, which is evident from Fig. S10(b) within the Supplemental Material [38]. Nonetheless, the J_{50} values for *p*-3CzBN, *o*-3CzBN, and *m*-3CzBN are lower than those of 5CzBN and 4CzBN, indicating a low EQE roll-off in them. These experimental behaviors can be understood from Case I, where a significant reduction of ϕ_D results in a reduction of efficiency roll-off. In addition, marginally lower peak EQEs (<5%) are observed for all three 3CzBN compounds, as predicted for Case I. It is also important to point out that there is a rapid drop in efficiency for *o*-3CzBN and *m*-3CzBN, exceeding current densities of 50 and 60 mA cm^{-2} , which might be due to the breakdown of the respective OLEDs. Interestingly, a comparison of 5CzBN and 4CzBN does not follow Case I, as 5CzBN demonstrates relatively lower efficiency roll-off, although it has higher ϕ_D and \bar{n}

TABLE I. Summary of decay rate constants and PL quantum efficiencies for mCP:4CzIPN and mCP:tri-PXZ-TRZ blend films.

TADF emitter	k_S ($\text{s}^{-1} \times 10^7$)	k_{ISC} ($\text{s}^{-1} \times 10^7$)	k_{RISC} ($\text{s}^{-1} \times 10^5$)	k_T ($\text{s}^{-1} \times 10^4$)	ϕ_{PL} (%)	ϕ_P (%)	ϕ_D (%)	ϕ_{ISC} (%)	ϕ_{RISC} (%)	\bar{n}
4CzIPN	3.0	4.1	5.9	9.5	84	41.9	42.1	58.1	72.5	1.00
tri-PXZ-TRZ	2.4	2.3	6.3	53	70	51.7	18.3	48.3	37.9	0.35

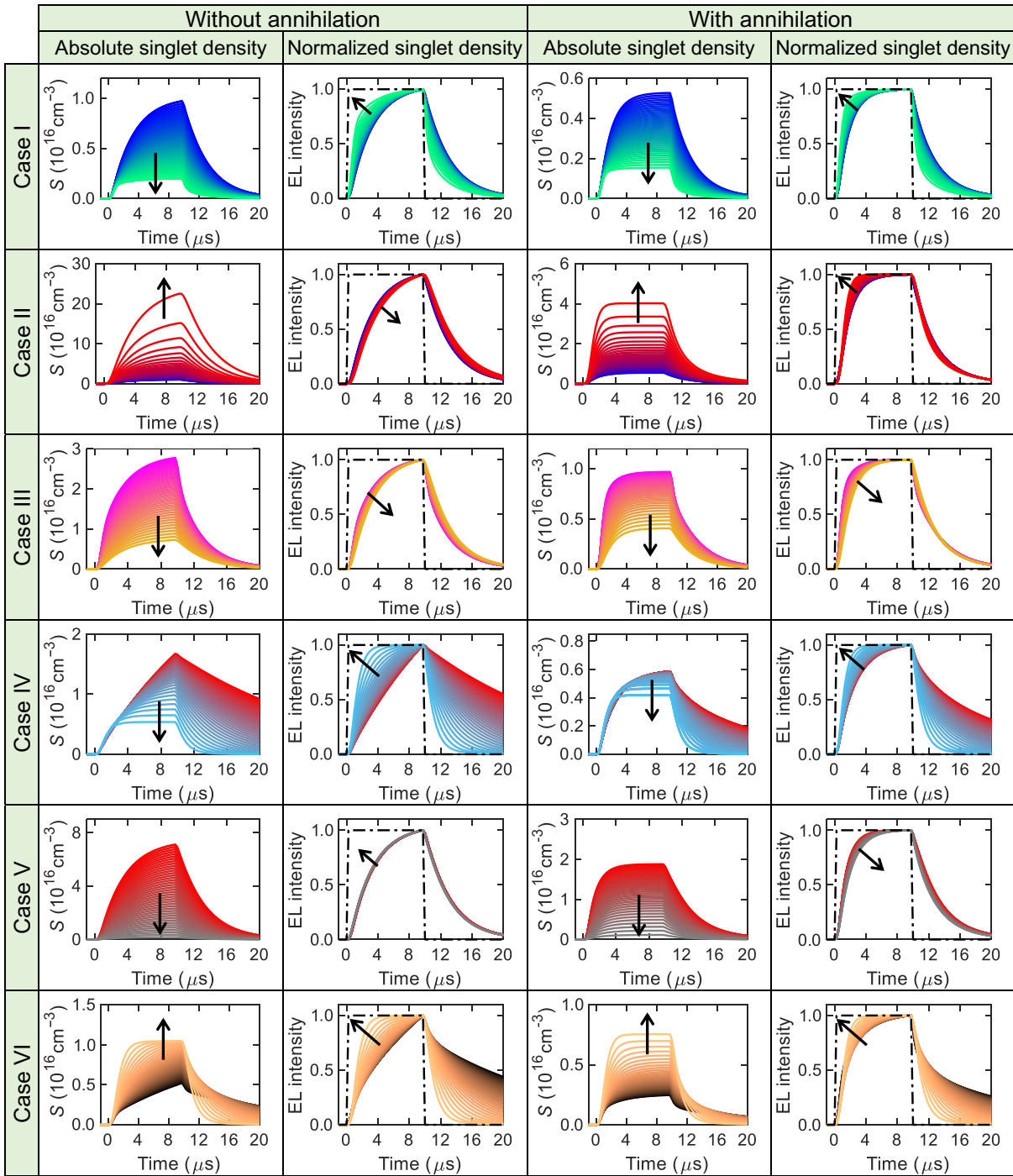


FIG. 8. Transient EL response. Calculated absolute singlet densities and corresponding normalized singlet densities as a function of time with and without annihilation conditions for Cases I–VI. Each row represents a case generated in this study. EL transients are calculated at a current density of 100 mA cm^{-2} . Note that the singlet exciton density in these figures is representative of the EL intensity. Solid arrows represent changes due to variations in decay rates and dashed-dotted lines represent the excitation pulse shape.

values compared to 4CzBN. The reason behind this lower EQE roll-off is primarily due to the shorter delayed lifetime in 5CzBN, which induces a fast RISC rate (an order higher than that of 4CzBN). This is attributed to less exciton quenching and lower efficiency roll-off, as

predicted for Case IV. Additionally, we analyze another TADF system, named 4PhCz2BN, reported by Mamada *et al.* [73]. The photophysical parameters for 50 wt % 4PhCz2BN doped in 3,3''-di(*9H*-carbazol-9-yl)-1,1''-biphenyl (mCBP) and neat films are listed in Table S5,

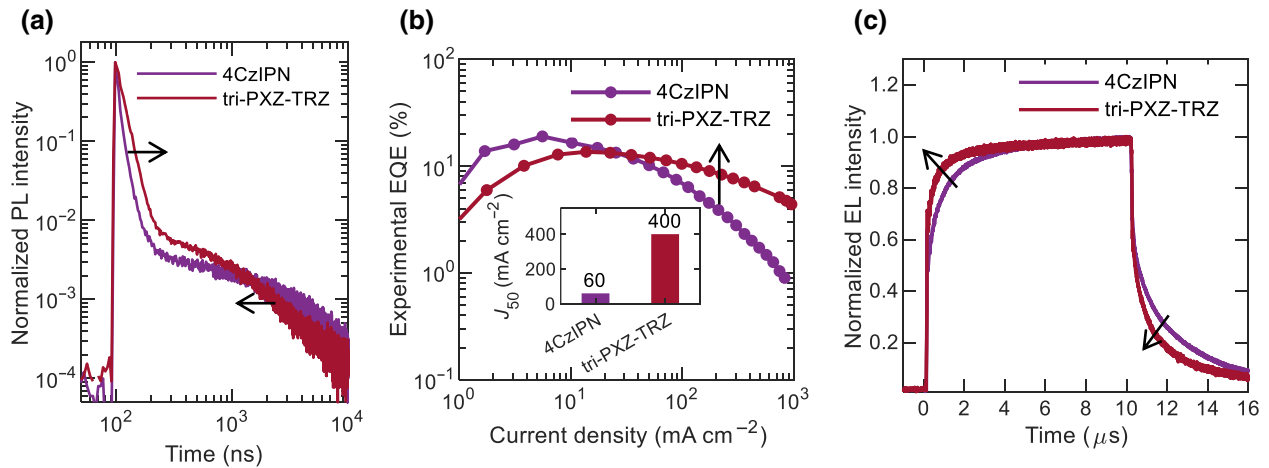


FIG. 9. Experimental analysis of (a) PL decay curves of 4CzIPN ($\tau_p = 14$ ns, $\tau_D = 2.9 \mu\text{s}$) and tri-PXZ-TRZ ($\tau_p = 21$ ns, $\tau_D = 1.2 \mu\text{s}$) doped in mCP host matrix. (b) EQE–current-density plot; inset, experimental J_{50} values. Low EQE roll-off behavior is observed for tri-PXZ-TRZ-based OLEDs. This EQE roll-off behavior can be explained from Case IV. (c) Normalized transient EL response.

and the corresponding EQE–current-density plots are shown in Fig. S12 within the Supplemental Material [38]. From Table S5 within the Supplemental Material [38], it can be seen that the conditions of both Case III and Case IV can be applied for the 50 wt % TADF blend, as both k_S and k_{RISC} are higher than those of the neat films. Therefore, a significant reduction in efficiency roll-off for 50 wt % doped OLEDs is observed compared to the neat devices.

IV. DISCUSSION

We investigate the role of the intrinsic photophysical parameters associated with exciton decay rates of TADF emitters, i.e., k_S , k_{ISC} , k_{RISC} , and k_T , and quantum efficiencies, i.e., ϕ_P , ϕ_D , ϕ_{ISC} , and ϕ_{RISC} , in optically excited decays, EQE roll-off, and transient ELs by considering a total of 240 TADF systems in six categories. Our results suggest a reduction in EQE roll-off while preserving a high maximum EQE is quite challenging due to the complex interplay between different deactivation channels in TADF. A high RISC rate may not necessarily reduce EQE roll-off if the contribution from the delayed component is high, with a long delayed lifetime or long prompt lifetime that gives rise to spin cycling. Both steady-state and transient EL studies indicate that one of the possible ways to reduce EQE roll-off and maintain a high maximum EQE is to improve the RISC rate by shortening the delayed lifetime and increasing the delayed contribution simultaneously. Besides the delayed component, the prompt component can also play a significant role in EQE roll-off behaviors, as shortening the prompt lifetime and increasing the prompt contribution can reduce EQE roll-off. In addition, TADF compounds exhibiting a short prompt lifetime and a long prompt contribution can also be

selected as the host to enhance the performance of TADF-assisted fluorescence OLEDs, also commonly known as hyperfluorescence (HF) OLEDs [66,74–76]. It is worth noting that either shortening the prompt lifetime or increasing the prompt contribution, or both, can result in an increase in k_S , which can amplify the Förster energy-transfer rate from the assisting TADF host to the fluorescent dopant in HF OLEDs.

ACKNOWLEDGMENTS

We thank the Australian Research Council (ARC, Grant No. DP200103036), Department of Industry, Innovation and Science (Grant No. AISRF53765), and the JSPS Core-to-Core Program (Grant No. JPJSCCA20180005) for financial support. M.H. is supported by the Australian Government’s Australian Postgraduate Award (APA). This work is performed, in part, at the Queensland node of the Australian National Fabrication Facility Queensland Node (ANFF-Q), a company established under the National Collaborative Research Infrastructure Strategy to provide nano- and microfabrication facilities for Australia’s researchers.

APPENDIX: EXPERIMENTAL METHODS

1. Photophysical measurements

UV-visible absorption and PL spectra of blend films are measured on quartz substrates using a Cary-5000 UV-Vis spectrophotometer and FS5 spectrofluorometer (Edinburgh Instruments), respectively. Time-correlated single-photon-counting measurements are performed with a Jobin-Yvon Fluorolog-3, by exciting the samples at an excitation wavelength of 372 nm generated by a pulsed LED and an instrument response of about 1 ns. The thin-film PL quantum yields are measured in a calibrated

integrating sphere under continuous nitrogen flow with a He-Cd laser as the excitation source (excitation wavelength = 325 nm).

2. OLED fabrication and characterization

The OLEDs are fabricated by using glass substrates with a 100-nm-thick prepatterned ITO layer purchased from Xinyan Technology Ltd. The substrates are cleaned by ultrasonication in Alconox solution, deionized water, acetone, and 2-propanol for 10 min in each solvent. Then the substrates are treated with UV-ozone for 30 min. Next, PEDOT:PSS (Ossila AI 4083) is then spin-coated at 4000 rpm (1 min) onto the substrates and annealed at 150 °C for 20 min. For emissive-layer deposition, solutions of the host and TADF emitters are prepared separately in chloroform and mixed to produce the blend solution with a concentration of 5 mg ml⁻¹. This mixed solution is spin-coated onto the PEDOT:PSS layer at 1500 rpm for 1 min under the N₂ atmosphere. The thickness of the spin-coated layers is determined by using a Dektak 150 profilometer. Finally, BP4mPy, LiF, and Al are deposited via thermal evaporation under vacuum ($\sim 10^{-7}$ mbar). All the steady-state current-density–voltage–luminance characteristics of the OLEDs are measured using Keithley 2400 source meters, a calibrated photomultiplier tube (PMT, Hamamatsu H10721-20), and a luminance meter (Konica Minolta LS100). The EQE is calculated (assuming Lambertian emission) using the brightness, current density, and emission spectrum of the device [77]. The transient EL responses are obtained by using a PMT (Hamamatsu H10721-20) connected to a digital oscilloscope (Teledyne LeRoy, 2 GHz). An AVTECH pulse generator (AVX1011-B1-B) with a short rise and fall time of <5 ns is used as the electrical excitation source for the transient EL measurements.

- [1] S.-J. Zou, Y. Shen, F.-M. Xie, J.-D. Chen, Y.-Q. Li, and J.-X. Tang, Recent advances in organic light-emitting diodes: Toward smart lighting and displays, *Mater. Chem. Front.* **4**, 788 (2020).
- [2] G. Hong, X. Gan, C. Leonhardt, Z. Zhang, J. Seibert, J. M. Busch, and S. Bräse, A brief history of OLEDs—emitter development and industry milestones, *Adv. Mater.* **33**, 2005630 (2021).
- [3] G. Huseynova, J.-H. Lee, Y. H. Kim, and J. Lee, Transparent organic light-emitting diodes: Advances, prospects, and challenges, *Adv. Opt. Mater.* **9**, 2002040 (2021).
- [4] H.-W. Chen, J.-H. Lee, B.-Y. Lin, S. Chen, and S.-T. Wu, Liquid crystal display and organic light-emitting diode display: Present status and future perspectives, *Light Sci. Appl.* **7**, 17168 (2018).
- [5] C. Murawski and M. C. Gather, Emerging biomedical applications of organic light-emitting diodes, *Adv. Opt. Mater.* **9**, 2100269 (2021).

- [6] C. Murawski, K. Leo, and M. C. Gather, Efficiency roll-off in organic light-emitting diodes, *Adv. Mater.* **25**, 6801 (2013).
- [7] H. Uoyama, K. Goushi, K. Shizu, H. Nomura, and C. Adachi, Highly efficient organic light-emitting diodes from delayed fluorescence, *Nature* **492**, 234 (2012).
- [8] T. Serevičius, J. Dodonova, R. Skaisgiris, D. Banovičius, K. Kazlauskas, S. Juršėnas, and S. Tumkevičius, Optimization of the carbazole–pyrimidine linking pattern for achieving efficient TADF, *J. Mater. Chem. C* **8**, 11192 (2020).
- [9] N. Acharya, M. Hasan, S. Dey, S.-C. Lo, E. B. Namdas, and D. Ray, Phenothiazine–quinoline conjugates realizing intrinsic thermally activated delayed fluorescence and room-temperature phosphorescence: Understanding the mechanism and electroluminescence devices, *Adv. Photonics Res.* **2**, 2000201 (2021).
- [10] U. Balijapalli, Y.-T. Lee, B. S. B. Karunathilaka, G. Tumen-Ulzii, M. Auffray, Y. Tsuchiya, H. Nakanotani, and C. Adachi, Tetrabenzof[*a,c*]phenazine backbone for highly efficient orange–red thermally activated delayed fluorescence with completely horizontal molecular orientation, *Angew. Chem., Int. Ed.* **60**, 19364 (2021).
- [11] N. Sharma, M. Maciejczyk, D. Hall, W. Li, V. Liégeois, D. Beljonne, Y. Olivier, N. Robertson, I. D. W. Samuel, and E. Zysman-Colman, Spiro-based thermally activated delayed fluorescence emitters with reduced nonradiative decay for high-quantum-efficiency, low-roll-off, organic light-emitting diodes, *ACS Appl. Mater. Interfaces* **13**, 44628 (2021).
- [12] D. Chen, Y. Kusakabe, Y. Ren, D. Sun, P. Rajamalli, Y. Wada, K. Suzuki, H. Kaji, and E. Zysman-Colman, Multichromophore molecular design for thermally activated delayed-fluorescence emitters with near-unity photoluminescence quantum yields, *J. Org. Chem.* **86**, 11531 (2021).
- [13] X. Wang, H. Li, X. Wu, H. Shu, H. Tian, H. Tong, and L. Wang, Highly efficient solution-processed thermally activated delayed fluorescence emitter based on a fused difluoroboron ketoiminate acceptor: C/N switch to realize the effective modulation of luminescence behavior, *J. Mater. Chem. C* **9**, 14133 (2021).
- [14] S. Dey, M. Hasan, A. Shukla, N. Acharya, M. Upadhyay, S.-C. Lo, E. B. Namdas, and D. Ray, Thermally activated delayed fluorescence and room-temperature phosphorescence in asymmetric phenoxazine–quinoline (D2–A) conjugates and dual electroluminescence, *J. Phys. Chem. C* **126**, 5649 (2022).
- [15] H. Lim, H. J. Cheon, S.-J. Woo, S.-K. Kwon, Y.-H. Kim, and J.-J. Kim, Highly efficient deep-blue OLEDs using a TADF emitter with a narrow emission spectrum and high horizontal emitting dipole ratio, *Adv. Mater.* **32**, 2004083 (2020).
- [16] A. Schinabeck, J. Chen, L. Kang, T. Teng, H. H. H. Homeier, A. F. Suleymanova, M. Z. Shafikov, R. Yu, C.-Z. Lu, and H. Yersin, Symmetry-based design strategy for unprecedentedly fast decaying thermally activated delayed fluorescence (TADF). Application to dinuclear Cu(I) compounds, *Chem. Mater.* **31**, 4392 (2019).
- [17] S.-J. Woo, Y. Kim, S.-K. Kwon, Y.-H. Kim, and J.-J. Kim, Phenazasiline/spiroacridine donor combined with methyl-substituted linkers for efficient deep blue thermally

- activated delayed fluorescence emitters, *ACS Appl. Mater. Interfaces* **11**, 7199 (2019).
- [18] B. Yurash, A. Dixon, C. Espinoza, A. Mikhailovsky, S. Chae, H. Nakanotani, C. Adachi, and T.-Q. Nguyen, Efficiency of thermally activated delayed fluorescence sensitized triplet upconversion doubled in three-component system, *Adv. Mater.* **34**, 2103976 (2022).
- [19] D. Rossi, D. Palazzo, A. Di Carlo, and M. Auf der Maur, Drift-diffusion study of the IQE roll-off in blue thermally activated delayed fluorescence OLEDs, *Adv. Electron. Mater.* **6**, 2000245 (2020).
- [20] S. Bangsund John, R. Van Sambeek Jack, M. Concannon Nolan, and J. Holmes Russell, Sub-turn-on exciton quenching due to molecular orientation and polarization in organic light-emitting devices, *Sci. Adv.* **6**, eabb2659 (2020).
- [21] M. Hasan, S. Saggar, A. Shukla, F. Bencheikh, J. Sobus, S. K. M. McGregor, C. Adachi, S.-C. Lo, and E. B. Namdas, Probing polaron-induced exciton quenching in TADF based organic light-emitting diodes, *Nat. Commun.* **13**, 254 (2022).
- [22] M. Hasan, A. Shukla, V. Ahmad, J. Sobus, F. Bencheikh, S. K. M. McGregor, M. Mamada, C. Adachi, S.-C. Lo, and E. B. Namdas, Exciton-exciton annihilation in thermally activated delayed fluorescence emitter, *Adv. Funct. Mater.* **30**, 2000580 (2020).
- [23] B. van der Zee, Y. Li, G.-J. A. H. Wetzelaer, and P. W. M. Blom, Origin of the efficiency roll-off in single-layer organic light-emitting diodes based on thermally activated delayed fluorescence, *Adv. Opt. Mater.* **9**, 2100249 (2021).
- [24] L.-K. Li, W.-K. Kwok, M.-C. Tang, W.-L. Cheung, S.-L. Lai, M. Ng, M.-Y. Chan, and V. W.-W. Yam, Highly efficient carbazolylgold(III) dendrimers based on thermally activated delayed fluorescence and their application in solution-processed organic light-emitting devices, *Chem. Sci.* **12**, 14833 (2021).
- [25] T. Ohsawa, H. Sasabe, T. Watanabe, K. Nakao, R. Komatsu, Y. Hayashi, Y. Hayasaka, and J. Kido, A series of imidazo[1,2-f]phenanthridine-based sky-blue TADF emitters realizing EQE of over 20%, *Adv. Opt. Mater.* **7**, 1801282 (2019).
- [26] Y. H. Lee, S. Park, J. Oh, S.-J. Woo, A. Kumar, J.-J. Kim, J. Jung, S. Yoo, and M. H. Lee, High-efficiency sky blue to ultradeep blue thermally activated delayed fluorescent diodes based on *ortho*-carbazole-appended triarylboron emitters: Above 32% external quantum efficiency in blue devices, *Adv. Opt. Mater.* **6**, 1800385 (2018).
- [27] M. Inoue, T. Serevius, H. Nakanotani, K. Yoshida, T. Matsushima, S. Juršnas, and C. Adachi, Effect of reverse intersystem crossing rate to suppress efficiency roll-off in organic light-emitting diodes with thermally activated delayed fluorescence emitters, *Chem. Phys. Lett.* **644**, 62 (2016).
- [28] H. Noda, X.-K. Chen, H. Nakanotani, T. Hosokai, M. Miyajima, N. Notsuka, Y. Kashima, J.-L. Brédas, and C. Adachi, Critical role of intermediate electronic states for spin-flip processes in charge-transfer-type organic molecules with multiple donors and acceptors, *Nat. Mater.* **18**, 1084 (2019).
- [29] B. H. Drummond, N. Aizawa, Y. Zhang, W. K. Myers, Y. Xiong, M. W. Cooper, S. Barlow, Q. Gu, L. R. Weiss, A. J. Gillett, *et al.*, Electron spin resonance resolves intermediate triplet states in delayed fluorescence, *Nat. Commun.* **12**, 4532 (2021).
- [30] V. V. Patil, H. L. Lee, I. Kim, K. H. Lee, W. J. Chung, J. Kim, S. Park, H. Choi, W.-J. Son, S. O. Jeon, and J. Y. Lee, Purely spin-vibronic coupling assisted triplet to singlet upconversion for real deep blue organic light-emitting diodes with over 20% efficiency and y color coordinate of 0.05, *Adv. Sci.* **8**, 2101137 (2021).
- [31] K. Traskovskis, A. Sebris, I. Novosjolova, M. Turks, M. Guzauskas, D. Volyniuk, O. Bezzivkonnyi, J. V. Grazulevicius, A. Mishnev, R. Grzibovskis, and A. Vembiris, All-organic fast intersystem crossing assisted exciplexes exhibiting sub-microsecond thermally activated delayed fluorescence, *J. Mater. Chem. C* **9**, 4532 (2021).
- [32] J. U. Kim, I. S. Park, C.-Y. Chan, M. Tanaka, Y. Tsuchiya, H. Nakanotani, and C. Adachi, Nanosecond-time-scale delayed fluorescence molecule for deep-blue OLEDs with small efficiency rolloff, *Nat. Commun.* **11**, 1765 (2020).
- [33] A. Endo, K. Sato, K. Yoshimura, T. Kai, A. Kawada, H. Miyazaki, and C. Adachi, Efficient up-conversion of triplet excitons into a singlet state and its application for organic light emitting diodes, *Appl. Phys. Lett.* **98**, 083302 (2011).
- [34] F. B. Dias, T. J. Penfold, and A. P. Monkman, Photophysics of thermally activated delayed fluorescence molecules, *Methods Appl. Fluoresc.* **5**, 012001 (2017).
- [35] Y. Wada, H. Nakagawa, S. Matsumoto, Y. Wakisaka, and H. Kaji, Organic light emitters exhibiting very fast reverse intersystem crossing, *Nat. Photonics* **14**, 643 (2020).
- [36] M. Lehnhardt, T. Riedl, T. Rabe, and W. Kowalsky, Room temperature lifetime of triplet excitons in fluorescent host/guest systems, *Org. Electron.* **12**, 486 (2011).
- [37] M. Li, M.-J. Sun, J. Yang, D. Huo, J. Lv, D. Shi, Y.-W. Zhong, and Y. Wan, Triplet-triplet energy transfer inside the single organic nanocrystal revealed by microscopic time resolved spectroscopy, *J. Phys. Chem. C* **126**, 11033 (2022).
- [38] See the Supplemental Material at <http://link.aps.org/supplemental/10.1103/PhysRevApplied.18.054082> for the supporting figures (Figs. S1–S12), supplemental note 1 for the calculation of host decay rates, and supplemental tables (Tables S1–S5) with all the experimental values used in this work.
- [39] D. Kasemann, R. Brückner, H. Fröb, and K. Leo, Organic light-emitting diodes under high currents explored by transient electroluminescence on the nanosecond scale, *Phys. Rev. B* **84**, 115208 (2011).
- [40] K. Masui, H. Nakanotani, and C. Adachi, Analysis of exciton annihilation in high-efficiency sky-blue organic light-emitting diodes with thermally activated delayed fluorescence, *Org. Electron.* **14**, 2721 (2013).
- [41] N. C. Erickson and R. J. Holmes, Engineering efficiency roll-off in organic light-emitting devices, *Adv. Funct. Mater.* **24**, 6074 (2014).
- [42] H. Nakanotani, H. Sasabe, and C. Adachi, Singlet-singlet and singlet-heat annihilations in fluorescence-based organic light-emitting diodes under steady-state high current density, *Appl. Phys. Lett.* **86**, 213506 (2005).
- [43] F. Bencheikh, A. S. D. Sandanayaka, T. Fukunaga, T. Matsushima, and C. Adachi, Origin of external quantum

- efficiency roll-off in 4,4'-bis[(n-carbazole)styryl]biphenyl (BSBCz)-based inverted organic light emitting diode under high pulsed electrical excitation, *J. Appl. Phys.* **126**, 185501 (2019).
- [44] A. Niwa, S. Haseyama, T. Kobayashi, T. Nagase, K. Goushi, C. Adachi, and H. Naito, Triplet-triplet annihilation in a thermally activated delayed fluorescence emitter lightly doped in a host, *Appl. Phys. Lett.* **113**, 083301 (2018).
- [45] T. Golubev, D. Liu, R. Lunt, and P. Duxbury, Understanding the impact of C_{60} at the interface of perovskite solar cells via drift-diffusion modeling, *AIP Adv.* **9**, 035026 (2019).
- [46] H. van Eersel, P. A. Bobbert, R. A. J. Janssen, and R. Coehoorn, Monte Carlo study of efficiency roll-off of phosphorescent organic light-emitting diodes: Evidence for dominant role of triplet-polaron quenching, *Appl. Phys. Lett.* **105**, 143303 (2014).
- [47] R. Coehoorn, L. Zhang, P. A. Bobbert, and H. van Eersel, Effect of polaron diffusion on exciton-polaron quenching in disordered organic semiconductors, *Phys. Rev. B* **95**, 134202 (2017).
- [48] R. Coehoorn, P. A. Bobbert, and H. van Eersel, Effect of exciton diffusion on the triplet-triplet annihilation rate in organic semiconductor host-guest systems, *Phys. Rev. B* **99**, 024201 (2019).
- [49] H. van Eersel, P. A. Bobbert, and R. Coehoorn, Kinetic Monte Carlo study of triplet-triplet annihilation in organic phosphorescent emitters, *J. Appl. Phys.* **117**, 115502 (2015).
- [50] B. Yurash, H. Nakanotani, Y. Olivier, D. Beljonne, C. Adachi, and T.-Q. Nguyen, Photoluminescence quenching probes spin conversion and exciton dynamics in thermally activated delayed fluorescence materials, *Adv. Mater.* **31**, 1804490 (2019).
- [51] H. Kaji, H. Suzuki, T. Fukushima, K. Shizu, K. Suzuki, S. Kubo, T. Komino, H. Oiwa, F. Suzuki, A. Wakamiya, *et al.*, Purely organic electroluminescent material realizing 100% conversion from electricity to light, *Nat. Commun.* **6**, 8476 (2015).
- [52] Y. Kondo, K. Yoshiura, S. Kitera, H. Nishi, S. Oda, H. Gotoh, Y. Sasada, M. Yanai, and T. Hatakeyama, Narrow-band deep-blue organic light-emitting diode featuring an organoboron-based emitter, *Nat. Photonics* **13**, 678 (2019).
- [53] H. J. Cheon, Y.-S. Shin, N.-H. Park, J.-H. Lee, and Y.-H. Kim, Boron-based multi-resonance TADF emitter with suppressed intermolecular interaction and isomer formation for efficient pure blue OLEDs, *Small* **18**, 2107574 (2022).
- [54] A. Monkman, Why do we still need a stable long lifetime deep blue OLED emitter?, *ACS Appl. Mater. Interfaces* **14**, 20463 (2022).
- [55] T. Hua, J. Miao, H. Xia, Z. Huang, X. Cao, N. Li, and C. Yang, Sulfone-incorporated multi-resonance TADF emitter for high-performance narrowband blue OLEDs with EQE of 32%, *Adv. Funct. Mater.* **32**, 2201032 (2022).
- [56] L.-S. Cui, A. J. Gillett, S.-F. Zhang, H. Ye, Y. Liu, X.-K. Chen, Z.-S. Lin, E. W. Evans, W. K. Myers, T. K. Ronson, *et al.*, Fast spin-flip enables efficient and stable organic electroluminescence from charge-transfer states, *Nat. Photonics* **14**, 636 (2020).
- [57] B. S. B. Karunathilaka, U. Balijapalli, C. A. M. Senevirathne, S. Yoshida, Y. Esaki, K. Goushi, T. Matsushima, A. S. D. Sandanayaka, and C. Adachi, Suppression of external quantum efficiency rolloff in organic light emitting diodes by scavenging triplet excitons, *Nat. Commun.* **11**, 4926 (2020).
- [58] X. Tang, U. Balijapalli, D. Okada, B. S. B. Karunathilaka, C. A. M. Senevirathne, Y.-T. Lee, Z. Feng, A. S. D. Sandanayaka, T. Matsushima, and C. Adachi, Electron-affinity substituent in 2,6-dicarbonitrile diphenyl-1λ5-phosphinine towards high-quality organic lasing and electroluminescence under high current injection, *Adv. Funct. Mater.* **31**, 2104529 (2021).
- [59] C. A. M. Senevirathne, S. Yoshida, M. Auffray, M. Yahiro, B. S. B. Karunathilaka, F. Bencheikh, K. Goushi, A. S. D. Sandanayaka, T. Matsushima, and C. Adachi, Recycling of triplets into singlets for high-performance organic lasers, *Adv. Opt. Mater.* **10**, 2101302 (2022).
- [60] I. Allison, H. Lim, A. Shukla, V. Ahmad, M. Hasan, K. Deshmukh, R. Wawrzinek, S. K. M. McGregor, J. K. Clegg, V. V. Divya, *et al.*, Solution processable deep-red phosphorescent Pt(II) complex: Direct conversion from its Pt(IV) species via a base-promoted reduction, *ACS Appl. Electron. Mater.* **1**, 1304 (2019).
- [61] R. Malmberg, T. von Arx, M. Hasan, O. Blacque, A. Shukla, S. K. M. McGregor, S.-C. Lo, E. B. Namdas, and K. Venkatesan, Tunable light-emission properties of solution-processable *N*-heterocyclic carbene cyclometalated gold(III) complexes for organic light-emitting diodes, *Chem. Eur. J.* **27**, 7265 (2021).
- [62] M. A. Baldo, D. F. O'Brien, Y. You, A. Shoustikov, S. Sibley, M. E. Thompson, and S. R. Forrest, Highly efficient phosphorescent emission from organic electroluminescent devices, *Nature* **395**, 151 (1998).
- [63] Q. Huang, S. Zhao, P. Wang, Z. Qin, Z. Xu, D. Song, B. Qiao, and X. Xu, Investigating the evolution of exciplex states in thermally activated delayed fluorescence organic light-emitting diodes by transient measurement, *J. Lumin.* **201**, 38 (2018).
- [64] A. Shukla, M. Hasan, G. Banappanavar, V. Ahmad, J. Sobus, E. G. Moore, D. Kabra, S.-C. Lo, and E. B. Namdas, Controlling triplet-triplet upconversion and singlet-triplet annihilation in organic light-emitting diodes for injection lasing, *Commun. Mater.* **3**, 27 (2022).
- [65] H. Tanaka, K. Shizu, H. Nakanotani, and C. Adachi, Twisted intramolecular charge transfer state for long-wavelength thermally activated delayed fluorescence, *Chem. Mater.* **25**, 3766 (2013).
- [66] H. Nakanotani, T. Higuchi, T. Furukawa, K. Masui, K. Morimoto, M. Numata, H. Tanaka, Y. Sagara, T. Yasuda, and C. Adachi, High-efficiency organic light-emitting diodes with fluorescent emitters, *Nat. Commun.* **5**, 4016 (2014).
- [67] B. Ruhstaller, S. A. Carter, S. Barth, H. Riel, W. Riess, and J. C. Scott, Transient and steady-state behavior of space charges in multilayer organic light-emitting diodes, *J. Appl. Phys.* **89**, 4575 (2001).
- [68] N. C. Giebink and S. R. Forrest, Quantum efficiency roll-off at high brightness in fluorescent and phosphorescent organic light emitting diodes, *Phys. Rev. B* **77**, 235215 (2008).

- [69] J. C. Scott, S. Karg, and S. A. Carter, Bipolar charge and current distributions in organic light-emitting diodes, *J. Appl. Phys.* **82**, 1454 (1997).
- [70] A. Shukla, V. Entoma, S. K. M. McGregor, M. Hasan, M. Mamada, E. G. Moore, C. Adachi, S.-C. Lo, and E. B. Namdas, Low light amplification threshold and reduced efficiency roll-off in thick emissive layer OLEDs from a diketopyrrolopyrrole derivative, *Macromol. Rapid Commun.* **43**, 2200115 (2022).
- [71] C. K. Vipin, A. Shukla, K. Rajeev, M. Hasan, S.-C. Lo, E. B. Namdas, A. Ajayaghosh, and K. N. N. Unni, White organic light-emitting diodes from single emissive layers: Combining exciplex emission with electromer emission, *J. Phys. Chem. C* **125**, 22809 (2021).
- [72] T. Hosokai, H. Matsuzaki, H. Nakanotani, K. Tokumaru, T. Tsutsui, A. Furube, K. Nasu, H. Nomura, M. Yahiro, and C. Adachi, Evidence and mechanism of efficient thermally activated delayed fluorescence promoted by delocalized excited states, *Sci. Adv.* **3**, e1603282 (2017).
- [73] M. Mamada, H. Katagiri, C.-Y. Chan, Y.-T. Lee, K. Goushi, H. Nakanotani, T. Hatakeyama, and C. Adachi, Highly efficient deep-blue organic light-emitting diodes based on rational molecular design and device engineering, *Adv. Funct. Mater.* **32**, 2204352 (2022).
- [74] N. R. Wallwork, M. Mamada, A. Shukla, S. K. M. McGregor, C. Adachi, E. B. Namdas, and S.-C. Lo, High-performance solution-processed red hyperfluorescent OLEDs based on cibalackrot, *J. Mater. Chem. C* **10**, 4767 (2022).
- [75] A. Shukla, S. K. M. McGregor, R. Wawrzinek, S. Saggar, E. G. Moore, S.-C. Lo, and E. B. Namdas, Light amplification and efficient electroluminescence from a solution-processable diketopyrrolopyrrole derivative via triplet-to-singlet upconversion, *Adv. Funct. Mater.* **31**, 2009817 (2021).
- [76] K. R. Naveen, H. Lee, R. Braventh, D. Karthik, K. J. Yang, S. J. Hwang, and J. H. Kwon, Achieving high efficiency and pure blue color in hyperfluorescence organic light emitting diodes using organo-boron based emitters, *Adv. Funct. Mater.* **32**, 2110356 (2022).
- [77] N. C. Greenham, R. H. Friend, and D. D. C. Bradley, Angular dependence of the emission from a conjugated polymer light-emitting diode: Implications for efficiency calculations, *Adv. Mater.* **6**, 491 (1994).